Electrostatic Effects on Proton Coupled Electron Transfer in Oxomanganese Complexes Inspired by the Oxygen-Evolving Complex of Photosystem II

Muhamed Amin,[†] Leslie Vogt,[‡] Serguei Vassiliev,[§] Ivan Rivalta,[‡,‖] Mohammad M. Sultan,[‡,⊥] Doug Bruce,[§] Gary W. Brudvig,[‡] Victor S. Batista,*[,‡] and M. R. Gunner*[,†]

[†]Department of Physics, City College of New York, New York, New York 10031, United States
[‡]Department of Chemistry, Yale University, New Haven, Connecticut 06520, United States
[§]Department of Biological Sciences, Brock University, St. Catherine, ON LS2 3A1, Canada

Ⓢ Supporting Information

ABSTRACT: The influence of electrostatic interactions on the free energy of proton coupled electron transfer in biomimetic oxomanganese complexes inspired by the oxygen-evolving complex (OEC) of photosystem II (PSII) are investigated. The reported study introduces an enhanced multiconformer continuum electrostatics (MCCE) model, parametrized at the density functional theory (DFT) level with a classical valence model for the oxomanganese core. The calculated pK_a's and oxidation midpoint potentials (E_m's) match experimental values for eight complexes, indicating that purely electrostatic contributions account for most of the observed couplings between deprotonation and oxidation state transitions. We focus on pK_a's of terminal water ligands in $[Mn(II/III)(H_2O)_6]^{2+/3+}$ (**1**), $[Mn(III)(P)(H_2O)_2]^{3-}$ (**2**, P = 5,10,15,20-tetrakis(2,6-dichloro-3-sulfonatophenyl)porphyrinato), $[Mn_2(IV,IV)(\mu\text{-}O)_2(terpy)_2(H_2O)_2]^{4+}$ (**3**, terpy = 2,2′:6′,2″-terpyridine), and $[Mn_3(IV,IV,IV)(\mu\text{-}O)_4(phen)_4(H_2O)_2]^{4+}$ (**4**, phen = 1,10-phenanthroline) and the pK_a's of μ-oxo bridges and Mn E_m's in $[Mn_2(\mu\text{-}O)_2(bpy)_4]$ (**5**, bpy = 2,2′-bipyridyl), $[Mn_2(\mu\text{-}O)_2(salpn)_2]$ (**6**, salpn = N,N′-bis(salicylidene)-1,3-propanediamine), $[Mn_2(\mu\text{-}O)_2(3,5\text{-}di(Cl)\text{-}salpn)_2]$ (**7**), and $[Mn_2(\mu\text{-}O)_2(3,5\text{-}di(NO_2)\text{-}salpn)_2]$ (**8**). The analysis of complexes **6−8** highlights the strong coupling between electron and proton transfers, with any Mn oxidation lowering the pK_a of an oxo bridge by 10.5 ± 0.9 pH units. The model also accounts for changes in the E_m's by ligand substituents, such as found in complexes **6−8**, due to the electron withdrawing Cl (**7**) and NO_2 (**8**). The reported study provides the foundation for analysis of electrostatic effects in other oxomanganese complexes and metalloenzymes, where proton coupled electron transfer plays a fundamental role in redox-leveling mechanisms.
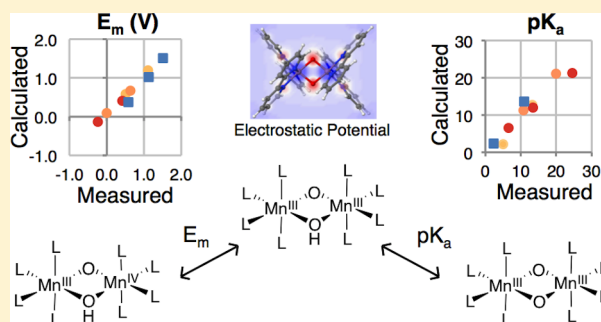
INTRODUCTION

Multinuclear metal ion clusters play important catalytic roles in a wide range of chemical and biological systems.[1−3] These clusters usually contain both protonatable and redox-active sites. They can carry out electroneutral oxidation state transitions by coupling electron and proton transfer reactions. The underlying redox leveling mechanism can greatly diminish the free energy needed to make reactive high valence redox states that are essential for multielectron reactions.[4−14] In general, understanding the electrochemistry of these metal centers and the coupling mechanism that tune the cluster chemistry is challenging. The thermodynamics of oxidation and deprotonation steps can be regulated by the core geometry and protonation states as well as by the charge distribution and protonation states of the ligands. Here, we focus on the analysis of the E_m's and pK_a's of a group of oxomanganese complexes inspired by the Mn_4O_5Ca cluster of the oxygen-evolving complex (OEC) of photosystem II (PSII).[15]

Many open questions about the OEC are common to both isolated and protein-embedded redox-active metal ion clusters.[16−18] These include: What is the nature of the oxidation state transition, and how does it change as a function of pH? Which acid−base/redox transitions are due to the inorganic core, and which ones are due to the influence of the ligands or the surroundings? What are the pK_a's of oxo bridges and terminal waters relative to each other, and how do they contribute to the deprotonation mechanism as a cluster is oxidized? A full, rigorous description of these processes is challenging and requires high level quantum mechanical treatments due to the importance of spin transitions, charge delocalization, Jahn−Teller distortion effects, and charge transfer interactions between Mn and the μ-O bridges. While several density functional theory (DFT) studies of oxomanganese clusters have been reported,[19−38] higher-level analyses
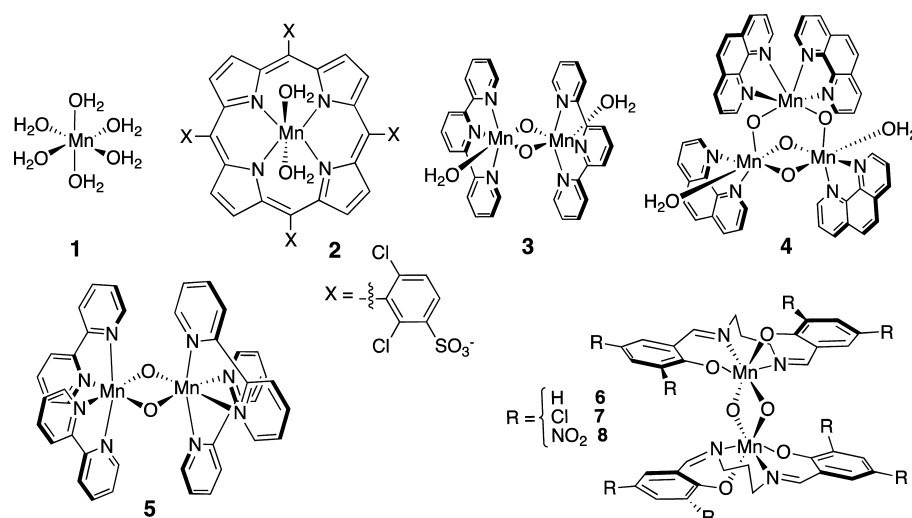
Figure 1. Model Mn complexes. (**1**) hexa-aqua Mn(II and III); (**2**) Mn(III) [5,10,15,20-tetrakis(2,6-dichloro-3-sulfonatophenyl)porphyrinato]$^{3-}$; (**3**) [Mn$_2$(IV,IV)(μ-O)$_2$(terpy)$_2$(H$_2$O)$_2$]$^{4+}$ (terpy = 2,2′:6′,2″-terpyridine); (**4**) [Mn$_3$(IV,IV,IV)(μ-O)$_4$(phen)$_4$(H$_2$O)$_2$]$^{4+}$ (phen = 1,10-phenanthroline); (**5**) [Mn$_2$(III,III; III,IV; and IV,IV)(μ-O)$_2$(bpy)$_4$] (bpy = 2,2′-bipyridyl); (**6−8**) [Mn$_2$(III,IV and IV,IV)(μ-O)$_2$(3,5-di(R)-salpn)$_2$], R = H (**6**), Cl (**7**), or NO$_2$ (**8**) (salpn = N,N′-bis(salicylidene)-1,3-propanediamine). Each porphyrinato and salpn unit has a charge of −2. The other ligands are neutral.

including more accurate descriptions of the multireference character of the electronic structures have yet to be reported.[39,40] Such treatments, however, remain rather difficult and time-consuming, even for single clusters with well-defined redox and protonation states. Multimetal center clusters, like the OEC, also present the challenge of evaluating a large number of possible states. For example, the OEC has four high-valent Mn centers in oxidation states III or IV, and five oxide bridges that can be either μ-hydroxo or μ-oxo, defining a total of 512 possible microstates. Furthermore, thousands of possible states need to be considered when including the possibility that some of the four terminal waters can also deprotonate. While the complexes analyzed in this paper are simpler than the OEC of PSII, they also involve a fairly large number of microstates. As an example, the dioxomanganese complex **5** (Figure 1) has sixteen possible formal charge configurations, including two states for each Mn (+3 or +4 charge), two for each oxide bridge (O^{2-} or OH$^-$), and one for the ligands. In addition, for clusters with terminal waters (**1−4**), each possible deprotonation of a terminal water into a hydroxo doubles the number of configurations. Therefore, the analysis of these complex clusters requires methods that can efficiently account for all oxidation and protonation states to understand how different configurations contribute to the redox properties that regulate the thermodynamics of the reaction.

Continuum electrostatic (CE) analysis, coupled to Monte Carlo methods as in the multiconformer continuum electrostatics (MCCE),[41] makes it possible to sample a large number of microstates to determine how redox midpoint potentials (E_m's) and pK_a's are modified by the surrounding environment.[41−43] However, these methods have generally been used to analyze nonbonded interactions. Here, we apply an enhanced MCCE method, parametrized at the DFT level, with a novel classical valence model for the oxomanganse core to study the electrostatic influence of ligands on proton-coupled oxidation reactions in oxomanganese complexes. The goal is to model the changes in interactions on redox and protonation changes between metals and the atoms in their first coordination sphere with a properly parametrized continuum

electrostatic analysis. We focus on the pK_a's of terminal waters in four complexes (hexa-aqua Mn, Mn porphyrin, di-Mn terpy, and tri-Mn phen) in oxidation states II−IV (complexes **1−4** in Figure 1). In addition, we study the pK_a's of the bridging oxygens in four dioxomanganese model complexes (complexes **5−8** Figure 1) and how the Mn redox state and ligand substitutions affect the pK_a's. The reported analysis provides fundamental insight into how changes in electrostatic interactions due to oxidation and protonation of the metal core or surrounding ligands affect the redox and protonation thermodynamics of oxomanganese cores inspired by the OEC of PSII.

METHODS

Enhanced MCCE Electrostatic Model. Complexes **1−8** are modeled by treating each Mn ion, oxide bridge, terminal water, and asymmetric unit of the organic ligand in a cluster as an individual gedanken fragment with an integer charge. The fragments interact with each other only via electrostatic and Lennard-Jones potentials. Microstates of the complexes are defined according to the oxidation states of the Mn fragments and the protonation states of the oxide bridges and/or terminal water ligands. The Boltzmann distribution of microstates is obtained by Monte Carlo (MC) sampling as a function of the solution's electron and proton chemical potential (i.e., E_h and pH) using the MCCE program.[41] These systems are small enough that all microstates could be enumerated to carry out full statistical mechanical calculations. However, the MC sampling is used in preparation for incorporating this valence analysis of metal clusters into proteins. The free energy of a microstate x, ΔG^x, is computed relative to the free energy of the separated fragments in a reference dielectric medium (e.g., water or acetonitrile (ACN)). ΔG^x is[41,44]

$$\Delta G^{x} = \sum_{i=1}^{M} \delta_{x,i} \{ [2.3 m_i k_B T (\text{pH} - \text{p}K_{a,sol,i})$$
$$+ n_i F (E_h - E_{m,sol,i})]$$
$$+ \Delta \Delta G_{solv,i} + \sum_{j=i+1}^{M} \delta_{x,i} [\Delta G_{ij}] \} \tag{1}$$

where M is the total number of states of all fragments; $\delta_{x,i}$ is 1 if fragment state i is present in the microstate and 0 otherwise; m_i is 1 (0) for the protonated (deprotonated) form of a bridging or terminal oxygen i; $k_B T$ is 25.37 meV at 298 K, the default temperature; n_i is the number of electrons gained using the most oxidized state as the reference state (1 for Mn(III) and 0 for Mn(IV) here); and F is the Faraday constant. $\text{p}K_{a,sol,i}$ and $E_{m,sol,i}$ are the reference $\text{p}K_a$ and E_m for the primitive fragment, i, in the reference solvent dielectric medium. Thus, the first and second terms in eq 1 establish the reference free energy changes of the isolated fragment due to protonation at the solution pH and/or reduction at the solution E_h (relative to the normal hydrogen electrode (NHE)).[45] The last two terms establish the changes in energy as the fragments are assembled into the cluster. CE interactions are computed with the Poisson−Boltzmann solver DelPhi[46] given input atomic positions, radii, and charges (Supporting Information S1). $\Delta \Delta G_{solv}$ is the loss of the CE solvation (reaction field) energy experienced by a fragment as it is moved from water or ACN into the cluster in that solvent. ΔG_{ij} is the pairwise electrostatic and Lennard-Jones interactions between fragments i and j present in the cluster microstate x. (Additional information about parameters required for the DelPhi CE analysis can be found in Supporting Information S1 and S6.)

Structural Models. Where possible, initial coordinates of complexes **1−8** are defined according to available crystal structures from the Cambridge Crystallographic Data Center (CCDC). Crystallographic solvent molecules and counterions are removed. Reference codes SAWYEU,[47] FIQFIU,[48] and SOZMUP[49] are used for **3**, **5**, and **6**, respectively. Structures are optimized at the DFT/B3LYP level of theory, using the LANL2DZ pseudopotential[50] for Mn and the 6-31G* basis set[51] for all other atoms, as implemented in GAMESS,[52] JAGUAR,[53] or Gaussian09.[54] In these initial structures, all terminal waters are neutral, bridging oxides are deprotonated, and Mn ions are set to the oxidation states Mn(III) or Mn(IV) using broken symmetry wave functions[55] for di-Mn complexes, as reported in previous work (Supporting Information S2).[22] The E_m's and $\text{p}K_a$'s derived using the Mn(III,IV) optimized geometries are used as the basis for the primary analysis. Values obtained with Mn(IV,IV) optimized structures are used to show how the outcome depends on the structure.

Atomic Partial Charges. In this model, integer formal charges are used for each fragment, and atomic positions are fixed. Mn atoms have a charge of +2, +3, or +4.

Each bridging oxygen has a formal charge of −2 in the deprotonated state. However, when protonated, a μ-hydroxo does not have the same charge distribution as a free OH⁻ due to interactions with the adjacent metal atoms. To account for this effect, atomic charges are adjusted to empirically reproduce the experimental $\text{p}K_a$ shift of 8.7 pH units in the $[\text{Mn}_2(\text{bpy})_4(\mu\text{-O})(\mu\text{-OH})]^{3+/4+}$ complex between the Mn(III,III) and Mn-(III,IV) states.[56] Using the DFT optimized Mn(IV,IV) structure, this $\Delta \text{p}K_a$ is recovered with a charge of −1.7 on oxygen and +0.7 on hydrogen (Supporting Information S3).

This charge distribution is used for all μ-hydroxo fragments regardless of solvent or microstate and is found to perform satisfactorily in all complexes.

Terminal waters have standard TIPS[57] partial charges, with a charge of −0.8 on the oxygen and +0.4 on each hydrogen. The terminal hydroxo has a net charge of −1 with charges of −1.2 on oxygen and +0.2 on hydrogen obtained by fitting the electrostatic potential of an isolated OH⁻ in water in a DFT calculation (B3LYP/6-31G*) with the polarizable continuum model (PCM) solvation model for bulk water in Gaussian09.[54]

A crucial element of the method is the use of quantum chemistry calculations to parametrize the atomic charge distribution of the organic ligands for subsequent classical electrostatic calculations. The atomic charges for all ligands except the terminal waters are fit to DFT-derived electrostatic potentials (ESP), subject to the constraint that the constituent fragments have integer total charges, as defined by their formal oxidation/protonation numbers. Ligand partial charges and atomic positions are held fixed in the MC sampling of cluster redox or protonation state. The charges are reported in Table S6 (Supporting Information) for each cluster.

To assign ligand charges, two rounds of DFT calculations are performed with B3LYP/LANL2DZ, 6-31G*.[51,58−61] First, ESP charges are obtained for the entire geometry-optimized cluster with all Mn in the Mn(IV) state. Then, ESP charges for an isolated ligand molecule with the appropriate net charge are determined with atom positions held fixed. The coordinated Mn is represented by a frozen fractional ESP charge, as determined in the entire complex, at the position found in the geometry-optimized full complex. The ligands parametrized are the porphyrin (**2**), terpy (**3**), phen (**4**), bpy (**5**), and salpn units (**6−8**). Each ligand fragment is given the same charge distribution; however, incorporating more than one ligand molecule into the fragment unit for charge determination does not change the outcome. The effect of charge transfer from the Mn into the ligand is included only implicitly through the distribution of ESP atomic charges within each fragment.

Reference Values of $E_{m,sol}$ and $\text{p}K_{a,sol}$. The reference values of midpoint potentials (E_m's) and $\text{p}K_a$'s for the gedanken constituent fragments in solution, $E_{m,sol}$ and $\text{p}K_{a,sol}$, are obtained according to the thermodynamic cycles for Mn and OH-bridges shown in Figure 2 (panels A and C, respectively). $E_{m,sol}$ and $\text{p}K_{a,sol}$ are constants that allow the calculated values to be compared to the reference NHE and solution pH. They do not affect the slope of the line that compares the experimental and calculated values in a given solvent, only the intercept. The experimental values E_m^{expt} and $\text{p}K_a^{expt}$ for one complex are used to derive the reference for all clusters. The $E_{m,sol}$ and $\text{p}K_{a,sol}$ are then used to calculate E_m's and $\text{p}K_a$'s in other clusters by computing the free energy of a microstate, according to eq 1.

The well-studied mixed-valence bpy complex **5** is used as the reference for the $E_{m,sol}$ in ACN. The measured reduction potential for $[\text{Mn}^{IV,IV}(\mu\text{-O})_2(\text{bpy})_4]^{4+}$ of 1.51 V versus NHE in ACN[62] is used as $E_{m,expt}$ (Figure 2A), giving a derived $E_{m,ACN}$ of 1.35 V for reduction of the isolated gedanken Mn. This $E_{m,ACN}$ is used to calculate the midpoint potential of all the di-Mn complexes, independent of the initial redox state or μ-oxo protonation pattern.

The reference $\text{p}K_{a,H_2O}$ of a terminal water is taken to be 15.7 (Supporting Information S4). The $\text{p}K_a$'s of terminal water ligands in the Mn complexes will be shifted due to electrostatic interactions within the cluster.
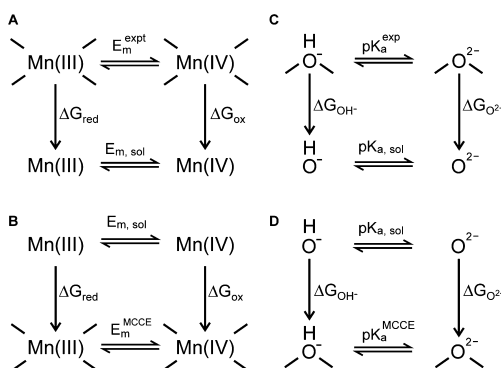
Figure 2. Thermodynamic cycles used to calculate the reference values of $E_{m,sol}$ (A) and $pK_{a,sol}$ (C) for the constituent Mn and hydroxo bridge fragments, using the experimental values E_m^{expt} and pK_a^{expt} for one cluster. The free energy differences in the cluster and isolated in solution, ΔG_{red}, ΔG_{ox}, ΔG_{OH^-}, and $\Delta G_{O^{2-}}$ for the gedanken fragments Mn(III), Mn(IV), OH^-, and O^{2-} are obtained by removing the interactions between the fragments as they are moved into solution. The derived $E_{m,sol}$ and $pK_{a,sol}$ are then used to calculate Mn E_m's (B) and bridging OH pK_a's (D) in other clusters.

Table 1. Calculated and Experimental pK_a's of Terminal Waters[a]

		pK_a^M	pK_a^C	error
$[Mn^{II}(H_2O)_6]^{2+}$	1	10.6^{64}	10.3	−0.3
$[Mn^{III}(H_2O)_6]^{3+}$	1	0.7^{64}	2.7	+2.0
$[Mn^{III}porphyrin(H_2O)_2]^{3-}$	2	4.4^{65}	4.9	+0.5
$[Mn_2^{IV}(\mu\text{-}O)_2(terpy)_2(H_2O)_2]^{4+}$	3	1.8^{66}	0.9	−0.9
$[Mn_3^{IV}(\mu\text{-}O)_4(phen)_4(H_2O)_2]^{4+}$	4	4.0^{67}	4.7	+0.7

[a]Numbers **1−4** refer to complexes detailed in Figure 1. The pK_a is listed for the first deprotonation in the cluster. pK_a^M: measured value. pK_a^C: calculated value. The geometry for each complex is optimized in the specified Mn redox state. The best-fit line comparing calculated and experimental values has a slope of 0.88, y-intercept of 0.91, and R^2 of 0.92 (Supporting Information Figure S4).

The $pK_{a,sol}$ for the loss of the proton from a hydroxo that represents the μ-oxo bridge is coupled to the calculation of the μ-OH^- charges. (Supporting Information S3). While water is the preferred solvent for benchmark values of clusters in proteins,[45] most reported values for μ-OH deprotonation in di-Mn clusters are measured in ACN. Here, one experimental value in each solvent is used to set the reference $pK_{a,sol}$. For water, the second deprotonation in the Mn(III,IV) state of complex **5**[37] is used to determine a pK_{a,H_2O} of 29.8 using the Mn(III,IV) optimized structure. The $pK_{a,ACN}$ is calculated to be 45.0 using a measured value for the first deprotonation of complex **6** in the Mn(IV,IV) state as a reference.[63] The derived $pK_{a,sol}$ for deprotonation of OH^- in water and ACN differs by 15.2 units.

■ RESULTS AND DISCUSSION

Benchmark Calculations of the pK_a's of Terminal Water Ligands. Table 1 reports the pK_a for deprotonation of terminal waters in complexes **1−4** as obtained with the enhanced MCCE methodology described in the Methods section. These calculations provide a stringent test of the MCCE methodology, as they are implemented with standard TIPS water atomic partial charges and the well established $pK_{a,sol}$ for bulk water of 15.7. The experimental pK_a's shift down by as much as 15 pH units when a water moves from bulk

solvent to become a Mn ligand. The comparison of calculated and experimental values shows a root-mean-square deviation (RMSD) of only 1.06 pH units (Supporting Information S4).

The pK_a shifts arising when a terminal water is bound to the Mn complex result from a balance of changes in electrostatic interactions between the Mn in the appropriate valence state, OH^- or H_2O, and the other ligands. The free energy changes can be decomposed into pairwise additive terms according to eq 1.[68] The interactions with each Mn center lower the pK_a of the titrating water, while interactions with the other waters (**1**), oxide bridges, and ligands (**2−4**) raise it. Interaction with the surrounding solvent is lost (desolvation penalty) when the ligand, Mn, or bridge is assembled into the cluster, which increases the pK_a. The effects of these changes are observed even for simple complexes, such as complex **1** ($[Mn^{II}(H_2O)_6]^{2+}$), for which the calculated pK_a of 10.3 is in good agreement with the experimental value of 10.6 (Table 1).[64] Here the shift of −5.4 pH units relative to bulk water represents a −7.4 kcal/mol net stabilization of the OH^- relative to bound water (1 pH unit is 1.367 kcal/mol). There is a +2.45 pH unit desolvation penalty reflecting the greater loss of the interaction with the solvent for the charged OH^- than the bound water. The pairwise electrostatic interactions with Mn^{II} stabilizes OH^- relative to the bound water by −9.4 pH units. Interactions of the OH^- with the other five waters arranged in octahedral coordination destabilize it by 1.54 pH units.

The enhanced MCCE method provides the pK_a or E_m shift when the gedanken fragments are moved from solution to the cluster. To go from a shift to a measurable pK_a or E_m, a reference $pK_{a,sol}$ or $E_{m,sol}$ for each titrating fragment must be determined in each solvent using the thermodynamic cycle shown in Figure 2. The experimental pK_a's and E_m's used to back-calculate $E_{m,sol}$ and $pK_{a,sol}$ using the cycles described in Figure 2A,C.

A $pK_{a,sol}$ of 29.8 for the μ-oxo bridge in water is obtained using the measured μ-oxo pK_a in complex **5**. The experimental pK_a in complex **6** provides a $pK_{a,sol}$ in ACN of 45.0. As water stabilizes the more highly charged O^{2-} state better than ACN, the $pK_{a,sol}$'s (and resultant cluster pK_a's) are lower in the more polar solvent. The same procedures are used to calculate the $E_{m,sol}$ of the Mn of 1.35 V in ACN using data from complex **5**. As all Mn E_m's were measured in ACN, only the $E_{m,sol}$ for this solvent can be determined.

Benchmark Calculations of E_m's and pK_a's of di-Mn Complexes. Figures 3−5 and Supporting Information Table S1 show the comparison of calculated and experimental values of eight E_m's and seven pK_a's for Mn centers and oxide bridges, respectively, in di-Mn complexes. The bpy (**5**) and salpn (**6−8**) complexes share a common oxygen-bridged dimanganese core that has been designed to explore the thermodynamic coupling between protonation and redox changes in high-valence Mn complexes. The pK_a's of these oxide bridges, spread over a 24 pH unit range, include measured data for the bpy complex (**5**) in water[56] and salpn (**6**, three values), Cl-salpn (**7**, two values), and NO_2-salpn (**8**, two values) in ACN.[63] Calculations using the DFT minimum energy configuration in the Mn(III,IV) state give an $R^2 \sim 0.95$ and a slope of 0.96. This uses a $pK_{a,ACN}$ = 45.0 (complexes **6−8**) and pK_{a,H_2O} = 29.8 (complex **5**) for deprotonation of the fragment OH^-. For data taken in a single solvent, $pK_{a,sol}$ does not affect the slope of a line comparing the experimental and calculated values. Rather, the reference $pK_{a,sol}$

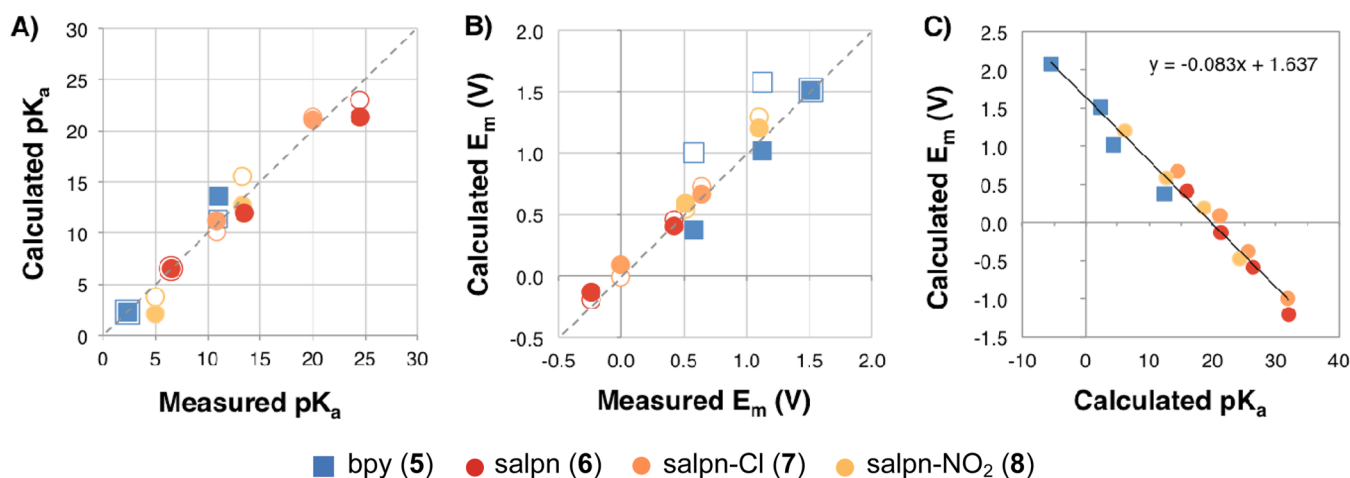**Figure 3.** Calculated versus experimental (A) pK_a's and (B) E_m's for bpy (**5**), salpn (**6**), and dichloro-(**7**) and dinitro-(**8**) substituted salpns. Calculations use structures optimized in the Mn(III,IV) (filled symbols) and the Mn(IV,IV) (open symbols) states. Data are from Figures 4 and 5 and Supporting Information Table S1. Dashed lines show an ideal correlation through the origin with a slope of 1. (A) pK_a's: The best-fit line with the Mn(III,IV) optimized structures has a slope of 0.96, y-intercept of −0.07 pH units, and R^2 of 0.9. Using structures optimized in the Mn(IV,IV) state, the line has a slope of 1.20, y-intercept of 26 mV, and R^2 of 0.92. (B) E_m's: The best-fit line with the Mn(III,IV) optimized structures has a slope of 0.99, y-intercept of −8 mV, and R^2 of 0.96. Using structures optimized in the Mn(IV,IV) state it has a slope of 1.1, y-intercept of 22 mV, and R^2 of 0.92. (C) Correlation between E_m's and pK_a's calculated with the Mn(III,IV) optimized structure for complexes **5**−**8** for oxidation or protonation reactions that increase the cluster charge by +1. Data are from Figures 4 and 5. The best-fit line has a slope of −83 mV/pK_a, y-intercept of 1.64 V, and R^2 of 0.97. All E_m's in all panels are calculated in ACN. All pK_a's are in ACN except for complex **5**, which is in water.
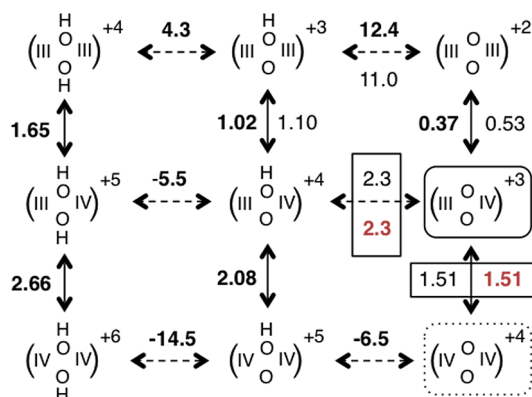

Figure 4. Calculated and experimental E_m's and pK_a's of bpy complex **5**. Each group in parentheses shows the redox state of the two Mn(III or IV) and the protonation state of the two bridging oxygens (OH⁻ as OH or O²⁻ as O). Calculated values of E_m's (V, bold, left of vertical arrows) compared to experimental data (light text, right of vertical arrows), and calculated (bold, above horizontal arrows) and experimental (below horizontal arrows) pK_a's for oxidation/deprotonation state transitions. The experimental values used to determine the reference $E_{m,sol}$ ($pK_{a,sol}$) are boxed. E_m's are given in ACN (solid arrows); pK_a's are in water (dashed arrows). Calculations are based on the fixed geometry optimized in the di-μ-oxo-Mn(III,IV) state (shown enclosed by a solid line). The fixed ligand charges are obtained in the symmetric di-μ-oxo-Mn(IV,IV) state (enclosed by a dotted line). Data from Supporting Information Tables S1 and S2.

determines the y-intercept, which is −0.07. With structures optimized in the Mn(IV,IV) state, the slope is 1.2.

The experimental E_m's (Figures 3−5 and Supporting Information Table 1 in S5) span 1.75 V and include data for bpy (**5**, two measured values[56,62,69]), salpn (**6**, two values), Cl-salpn (**7**, two values), and NO₂-salpn (**8**, two values).[63] There is a very good agreement between calculated and experimental data using the Mn(III,IV) structures. The linear fit gives a slope of 0.99, RMSD of 70 mV, and R^2 of 0.96.[70] With an $E_{m,ACN}$ =

1.35 V, the y-intercept is −8 mV. As for the analysis of pK_a's, calculations of E_m's based on the Mn(IV,IV) structures (open symbols in Figure 3B) gives a less satisfactory slope of 1.1.

The enhanced MCCE model greatly simplifies the analysis of the oxo-Mn clusters. The E_m and pK_a changes in different clusters are solely controlled by the classical electrostatic energies between the Mn, the bridging oxygens, and the first coordination shell ligands. A valence integer charge is assigned to each fragment that changes charge in the analysis. The DFT input provides cluster geometry and ligand charges that are parametrized in a single state and do not change with the reaction. Yet this simple model does a remarkable job of capturing the experimental E_m's and pK_a's for this group of complexes.

Predicted E_m's and pK_a's. Complexes **5**−**8** are well studied.[56,63,70,71] However, due to the intrinsic instability of oxomanganese complexes and other experimental limitations, measurements cannot provide a full picture of the electrochemistry of these complexes. Figures 4 and 5 show that there are six E_m's and six pK_a's associated with possible transitions in each cluster from the (top, left) di-μ-hydroxo-Mn(III,III) state to the (bottom, right) di-μ-oxo-Mn(IV,IV) state. Of the twelve possible values, only four or five have been measured for each of complexes **5**−**8**. Here, we predict all E_m's and pK_a's in these clusters. These values are used to gain a better insight into the manner in which the changes in the ligands or the protonation or redox state change the electron and proton transfer thermodynamics.

The unmeasured values of the E_m's and pK_a's of the bpy complex **5** (Figure 4) and the salpn complexes **6**−**8** (Figure 5) are predicted in the structures optimized in the Mn(III,IV) state. For comparison, calculations based on the Mn(IV,IV) geometries are also reported in the Supporting Information (Table 2 in S5). Using both measured and predicted values, the analysis can provide an overview of how changes in redox and protonation states shift subsequent reactions in a complex and
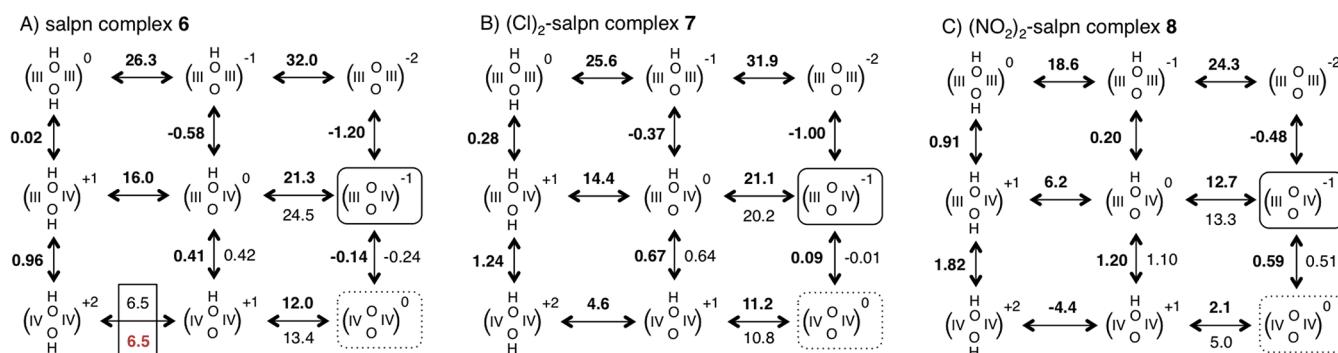
Figure 5. Calculated and experimental E_m's and pK_a's in ACN of salpn complexes **6**−**8**. See Figure 4 for full description.

Table 2. Shifts in E_m's and pK_a's Induced by Changes in the Charge Distribution of the Ligands, Protonation States of Oxide Bridges, or Oxidation State Transitions in the Mn Dimer Complexes 5−8[a]

	$pK_a(\mu\text{-}O)$	$E_m(Mn)$ (V)
ligand charge distribution		
with Cl substituents[b]	−0.9 ± 0.7	+0.22 ± 0.03
with NO_2 substituents[c]	−9.1 ± 1.3	+0.80 ± 0.07
protonation of μ-O[d]	−6.1 ± 0.5	+0.60 ± 0.06
oxidation of Mn[d]	−10.6 ± 0.9	+1.01 ± 0.08
net ligand charge ($-2 \to 0$)[e]	−13.6 ± 1.4	+1.68 ± 0.09

[a]Average of appropriate calculated values for complexes **5**−**8** in ACN using Mn(III,IV) geometries. [b]Complex **7** vs **6**. [c]Complex **8** vs **6**. [d]Comparison of pK_a or E_m values for complexes **5**−**8** with different bridging oxygen protonation. [e]Comparison of six pK_a's or six E_m's for complex **6** vs **5**. Data from Figures 4 and 5.

how changing the ligands alters the free energy of electron and proton transfer in different complexes (Table 2).

Solvent Effects on pK_a's. Many of the manganese model complexes studied here are unstable in water. Special techniques are required to stabilize the complexes in aqueous solutions, such as the use of buffer solutions (most commonly acetate or phosphate) with an excess of ligand. Therefore, most measurements of E_m's and pK_a's have been performed in nonaqueous solutions. For complex **6**, experimental pK_a's for the bridging oxygens were measured only in ACN solution. The pK_a's are predicted in water by changing the solvent dielectric constant around the fragments or the cluster from 40 for ACN to 80 for water and changing the reference $pK_{a,sol}$ for the gedanken, O from the value determined in ACN (45.0) to that determined in water (29.8). The six calculated pK_a's are 6.7 ± 0.9 pH units lower in water than in ACN. The calculated pK_a shifts are consistent with measurements of other hydrido transition metal complexes that have reported a shift of about 7.5 pH units when comparing pK_a's in water and in ACN.[72] The similarity of the solvent-induced pK_a shift found for other transition metal complexes provides support for the predictions using the enhanced MCCE method and gives insight into the crucial role played by the surrounding medium on the acid−base/redox properties of oxomanganese complexes. The ability to approximate how pK_a's measured in ACN will shift in water allows clearer comparison with the properties of oxomanganese complexes embedded in aqueous biological environments.

Ligand Effects on pK_a's and E_m's. Another important question is how well the method introduced here captures the effect of changing the ligand net change and charge distribution on the E_m's and pK_a's. For example, a comparison of Figures 4

and **5** (panel A) shows a dramatic increase in the six μ-oxo pK_a's by 20.2 ± 1.4 pH units when the neutral bpy ligands (**5**) are exchanged by salpn (with a net charge of −2) in complex **6**. Part of the μ-oxo pK_a shift (6.7 pH units) is due to the change of solvent, as described above. The other 13.6 pH units, however, is caused by the anionic ligands raising the μ-oxo pK_a's in the cluster. The ligand charges also affect the redox potentials of the Mn centers that undergo a large change when the bpy ligands (**5**) are exchanged by the salpn (**6**) (Figure 4 and panel A in Figure 5). Comparing the six E_m's in cluster **5** with those in **6** shows a shift of 1.68 ± 0.09 V. The small standard deviation suggests that the influence of the anionic ligand is similar for all redox and protonation states of these complexes. Knowledge of the magnitude of these shifts is particularly important for understanding biological complexes such as the OEC of PSII, where the ligation of the oxomanganese by several anionic groups, including the carboxylates of Asp and Glu side chains of surrounding amino acid residues, will be expected to modify the thermodynamics of oxidation and deprotonation reactions.[73]

Ligand substituent groups can also regulate the E_m's and pK_a's. In the method used here, this influence is accounted for by changing the atomic partial charge distribution on the ligand, which changes the electrostatic potential at the Mn centers and bridging oxides. The three salpn complexes **6**−**8** have the same ligand net charge yet they show significant polarization effects induced by the electron withdrawing groups in the salpn ligands (Figures 5 and 6 and Supporting Information S5 and S6). Where there are available data, the calculated pK_a's and E_m's
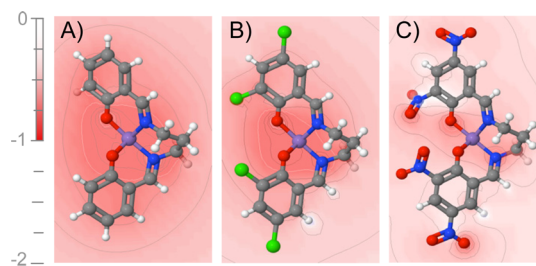

Figure 6. Slices of the DFT electrostatic potential from each ligand in complexes (A) **6**, (B) **7**, and (C) **8** in the plane which contains the axial ligand atoms and is perpendicular to the $[Mn_2(\mu\text{-}O)_2]$ core (zero-charge Mn atom location shown in purple). The electron-withdrawing substituents Cl and NO_2 move electron density from around Mn to above and below the plane shown here, shifting the redox potential to more positive values (see Supporting Information S8 for ligand charges and S6 for the correlation between N atom charges and cluster E_m and pK_a).

match the values for these complexes, which shows the electrostatic potential model can adequately describe the influence of the charge redistribution induced by electron withdrawing substituents. Considering all predicted values, the Cl substitution shifts the μ-O pK_a by -0.9 ± 0.7 pH units and the E_m by $+0.22 \pm 0.03$ V, while NO$_2$ substitution shifts the pK_a by -9.1 ± 1.3 pH units and the E_m by $+0.8 \pm 0.07$ V.

The E_m's and pK_a's in complexes **5–8** shift in a regular manner when the net charge of the complex is changed by protonation or oxidation of the oxygen-bridged dimanganese core. For example, protonating an oxide bridge shifts the pK_a of the second μ-O bridge pK_a to be -6.1 ± 0.5 pH units lower than the first one. Each added proton shifts the Mn E_m up by $+0.60 \pm 0.06$ V. Similarly, starting in the Mn(III,III) state, oxidation of the first Mn(III) raises the electrostatic potential of the inorganic core, making the oxidation of the second Mn(III) $+1.01 \pm 0.08$ V harder. The pK_a of the oxide bridge shifts by -10.6 ± 0.9 pH units with each Mn oxidation. Remarkably, these changes are accounted for by the changes in formal charges of the Mn and oxide fragments because the current model neglects changes in the ligand charges or cluster geometry induced by oxidation/protonation state transitions.

Dependence on the Input Structure. The empirical method presented here is sensitive to the atomic positions in the structure. The E_m's and pK_a's for complex **5** were calculated with structures subjected to DFT geometry optimization in the Mn(III,IV) and Mn(IV,IV) states with singly protonated or deprotonated oxo bridges (Supporting Information Table 3 in S5). Protonation of the μ-oxo bridge increases the Mn(IV)–O bond length by 0.11 Å and the Mn(III)–O by 0.57 Å in the Mn(III,IV) structure. In the Mn(IV,IV) structure, the Mn-(IV)–O bond increases by 0.15 Å. The longer bonds reduce the electrostatic interaction between the oxide bridge and the Mn center and shift the calculated pK_a's and E_m's. However, calculations starting with structures optimized in the same redox and protonation state show regular shifts in the pK_a's and E_m's. For example, protonation of one oxygen bridge increases the calculated pK_a of the second bridge by 12.1 ± 2.7 for the Mn(III,IV) structure and 12.3 ± 2.4 for the Mn(IV,IV) structure. The calculations with Mn(III,IV) structures provide a better match to the experimental data than those carried out with the geometry optimized in the Mn(IV,IV) (Figure 3A,B) or Mn(III,III) state (data not shown). Since we use the same atomic charge values in all cases, it is the position of the ligand atoms that results from the Jahn–Teller distortion around the high-spin Mn(III) center(s), which is captured by the DFT-derived geometries that change when the structures are optimized in different states. Consistent with this picture, the effect of point charge location is most apparent for the neutral ligands of complex **5**, where the E_m values are too high when the Mn(IV,IV) structure is used Figure 3B, open squares). Thus, in an empirical method such as that used here, good agreement with experimental results relies on the use of consistent methods to define the structures, partial charges, and reference p$K_{a,sol}$ and $E_{m,sol}$ for all complexes.

Thermodynamic Coupling in Dioxomanganese Complexes. The correlated shifts of E_m's and pK_a's found by the MCCE analysis (Figure 3C) shows that the $[Mn_2(\mu-O)_2]$ core responds as a unit to changes in electrostatic interactions. This results in a strong correlation between changes in the Mn redox potential and changes in the oxide bridge pK_a in all complexes. The cluster charge can be increased by $+1$ by either Mn oxidation or cluster protonation. MCCE predicted values show

a correlation of E_m's and pK_a's for a given cluster state with a slope of $\sim$83 mV/pK_a unit (Figure 3C). This is in quantitative agreement with experimental studies by Pecoraro and co-workers, where a slope of 85 mV/pK_a unit was found.[70]

The underlying changes in protonation and oxidation states compared in Figure 3C represent independent, *uncoupled*, processes. Figure 3C analyzes reactions involving a step along the horizontal direction and another step vertically in Figures 4 and 5 and Supporting Information S7. The correlation is thus significantly different from the dependence of E_m with pH in PCET mechanisms, as in the reaction

$$[Mn^{IV}(\mu\text{-}O)_2 Mn^{IV}] + e^- + H^+$$
$$\rightleftarrows [Mn^{III}(\mu\text{-}O)(\mu\text{-}OH)Mn^{IV}]$$
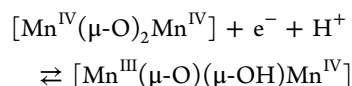
where the E_m must change by 59 mV/pH unit.

Thus, PCET corresponds to transitions along the diagonal. In both sequential and tightly coupled electron and proton transfer reactions, deprotonation increases the basicity of the bridge and, therefore, lowers the potential for oxidation of the complex. These mechanisms are thus essential to stabilize high-valent (nonoxidizing) states that can accumulate several oxidation equivalents before engaging in redox reactions.

Potential Lessons for Proton Release with Oxidation of the OEC of PSII. Complexes **3** and **5–8** have been constructed as models of the OEC of PSII which is thought to evolve along the catalytic water splitting cycle from the most reduced S_0 state (Mn(III,III,III,IV)) to the S_3 state (Mn-(IV,IV,IV,IV)), before forming an oxyl radical species responsible for the O–O bond formation.[74] The results reported in Table 2 and Figures 4 and 5 provide information that can help understand the OEC Mn$_4$O$_5$Ca cluster. The analysis of the oxomanganese clusters shows that the pK_a of oxo bridges shifts by 9–10 pH units each time the complex is oxidized, making them good candidates to lose a proton each time the Mn core is oxidized, as long as any bridging oxygens remain protonated.[16] A close coupling between the core losing protons and electrons is generally consistent with earlier computational models of the OEC that combined DFT and QM/MM models[20,23,75,76] of the S_0 and S_1 states. These earlier simulations suggest that the last deprotonation of an OEC hydroxo bridge occurs during the formation of the S_1 state, with two Mn^{III} and two Mn^{IV} centers and all bridging oxygens in the μ-oxo form.[77] The question remains as to whether protons are then lost from a terminal water when going to the S_2 state,[20] especially since there is no proton release to the lumen at physiological pH in this transition.[78] HYSCORE experiments do suggest that there are no terminal hydroxo ligands in the S_2 state,[79] while a recent DFT study suggests that one of the terminal water ligands is deprotonated.[27] Notably, the proposed electrostatic valence model will be able to explore the variations of pK_a's and E_m's of the OEC as a function of the protonation states of vicinal amino acid residues (e.g., D61, H337, R357) and replacement of cofactors, such as chloride[80] or calcium. Such applications could shed light on the several structure–function relations in PSII.

■ CONCLUSIONS

We have documented for the first time the capabilities and limitations of an enhanced MCCE methodology to characterize proton-coupled electron transfer in oxomanganese complexes using MC sampling of protonation and redox states on the same footing.[80,81] The methodology provides predictions with

RMSD of 70 mV for E_m's covering a 1.75 V range, and a 2 pH unit RMSD for pK_a's over a 24 pH unit range, without preassignment of the microstate at the outset of the calculation as is usually done in other techniques, such as standard molecular dynamics, DFT, or QM/MM analysis. The MCCE method, thus, bypasses the exponential scaling problem, due to the large number of possible microstates, and allows for an efficient assessment of the sequence of oxidation and deprotonation state transitions for multicenter redox/acid—base cofactor chelated by Lewis base ligands and surrounded by a cluster or protein environment. The calculations show a remarkable ability of the MCCE methodology to predict shifts in Mn E_m's and pK_a's of hydroxo bridges and terminal water ligands in a series of complexes parametrized by geometries and partial atomic charges from quantum chemistry calculations. The E_m and pK_a shifts are modeled solely by the changes in the CE interactions between the Mn and the atoms in their first coordination shell.

Given the success of this simple analysis, the methodology can now be extended and applied to the study of other biologically important Mn complexes such as superoxide dismutase[82] and the OEC of PSII.[16,83] The reported enhanced MCCE analysis of trends of redox potentials and pK_a's across several complexes and solvents partially validate the classical electrostatic methodology as capable of accounting for changes in the electrostatic potential at the positions of the redox/acid—base constituent fragments. The analysis also provides guidelines for ligand design that should be useful to modulate redox/acid—base transitions.

ASSOCIATED CONTENT

$\mathbf{S}$ Supporting Information

Figure of the complexes; parameters for determining the microstate energies; input structure; empirical method for assigning the partial charge distribution on the μ-oxo bridges; values for calc vs exp pK_a and E_m; correlation between the total charges on the atoms ligating the Mn ions and the E_m and pK_a shift; figure for terminal water pK_a calc vs exp. This material is available free of charge via the Internet at http://pubs.acs.org.

AUTHOR INFORMATION

Corresponding Author
*M.R.G., gunner@sci.ccny.cuny.edu; V.S.B., victor.batista@yale.edu.

Present Addresses
‖Dipartimento di Chimica "G. Ciamician", Università di Bologna, V. F. Selmi 2, 40126 Bologna, Italy.
⊥Department of Chemistry, Stanford University, 333 Campus Dr., Mudd Building, Room 121, Stanford, California 94305-4401, U.S.A.

Notes
The authors declare no competing financial interest.

ACKNOWLEDGMENTS

REFERENCES

(1) David, S. S.; Meggers, E. Inorganic Chemical Biology: from Small Metal Complexes in Biological Systems to Metalloproteins. Curr. Opin. Chem. Biol. 2008, 12, 194−196.

(2) Lindh, U. Metal Biology: Aspects of Beneficial Effects. Ambio 2007, 36, 107−110.

(3) Holm, R. H.; Kennepohl, P.; Solomon, E. I. Structural and Functional Aspects of Metal Sites in Biology. Chem. Rev. 1996, 96, 2239−2314.

(4) Mayer, J. M. Proton-Coupled Electron Transfer: A Reaction Chemist's View. Annu. Rev. Phys. Chem. 2004, 55, 363−390.

(5) Mayer, J. M.; Rhile, I. J. Thermodynamics and Kinetics of Proton-Coupled Electron Transfer: Stepwise vs. Concerted Pathways. Biochim. Biophys. Acta, Proteins Proteomics 2004, 1655, 51−58.

(6) Auer, B.; Fernandez, L. E.; Hammes-Schiffer, S. Theoretical Analysis of Proton Relays in Electrochemical Proton-Coupled Electron Transfer. J. Am. Chem. Soc. 2011, 133, 8282−8292.

(7) Cukier, R. I.; Nocera, D. G. Proton-Coupled Electron Transfer. Annu. Rev. Phys. Chem. 1998, 49, 337−369.

(8) Fecenko, C. J.; Thorp, H. H.; Meyer, T. J. The Role of Free Energy Change in Coupled Electron-Proton Transfer. J. Am. Chem. Soc. 2007, 129, 15098−15099.

(9) Hammes-Schiffer, S. Theoretical Perspectives on Proton-Coupled Electron Transfer Reactions. Acc. Chem. Res. 2001, 34, 273−281.

(10) Hammes-Schiffer, S. Introduction: Proton-Coupled Electron Transfer. Chem. Rev. 2010, 110, 6937−6938.

(11) Hammes-Schiffer, S.; Hatcher, E.; Ishikita, H.; Skone, J. H.; Soudackov, A. V. Theoretical Studies of Proton-Coupled Electron Transfer: Models and Concepts Relevant to Bioenergetics. Coord. Chem. Rev. 2008, 252, 384−394.

(12) Hammes-Schiffer, S.; Iordanova, N. Theoretical Studies of Proton-Coupled Electron Transfer Reactions. Biochim. Biophys. Acta, Proteins Proteomics 2004, 1655, 29−36.

(13) Hammes-Schiffer, S.; Soudackov, A. V. Proton-Coupled Electron Transfer in Solution, Proteins, and Electrochemistry. J. Phys. Chem. B 2008, 112, 14108−14123.

(14) Hammes-Schiffer, S.; Stuchebrukhov, A. A. Theory of Coupled Electron and Proton Transfer Reactions. Chem. Rev. 2010, 110, 6939−6960.

(15) Manchanda, R.; Brudvig, G. W.; Crabtree, R. H. High-Valent Oxomanganese Clusters: Structural and Mechanistic Work Relevant to the Oxygen-Evolving Center in Photosystem II. Coord. Chem. Rev. 1995, 144, 1−38.

(16) McEvoy, J. P.; Brudvig, G. W. Water-Splitting Chemistry of Photosystem II. Chem. Rev. 2006, 106, 4455−4483.

(17) Cady, C. W.; Crabtree, R. H.; Brudvig, G. W. Functional Models for the Oxygen-Evolving Complex of Photosystem II. Coord. Chem. Rev. 2008, 252, 444−455.

(18) Brudvig, G. W.; Beck, W. F.; de Paula, J. C. Mechanism of Photosynthetic Water Oxidation. Annu. Rev. Biophys. Biophys. Chem. 1989, 18, 25−46.

(19) Leung, K.; Rempe, S. B.; Schultz, P. A.; Sproviero, E. M.; Batista, V. S.; Chandross, M. E.; Medforth, C. J. Density Functional Theory and DFT+U Study of Transition Metal Porphines Adsorbed on Au(111) Surfaces and Effects of Applied Electric Fields. J. Am. Chem. Soc. 2006, 128, 3659−3668.

(20) Luber, S.; Rivalta, I.; Umena, Y.; Kawakami, K.; Shen, J. R.; Kamiya, N.; Brudvig, G. W.; Batista, V. S. S_1-State Model of the O_2-Evolving Complex of Photosystem II. Biochemistry 2011, 50, 6308−6311.

(21) McEvoy, J. P.; Gascon, J. A.; Sproviero, E. M.; Batista, V. S.; Brudvig, G. W. In *Photosynthesis: Fundamental Aspects to Global Perspectives*; Bruce, D., van der Est, A., Eds.; Allen Press: Lawrence, KS, 2005; Vol. *1*, pp 278−280.

(22) Sproviero, E. M.; Gascon, J. A.; McEvoy, J. P.; Brudvig, G. W.; Batista, V. S. Characterization of Synthetic Oxomanganese Complexes and the Inorganic Core of the O_2-evolving Complex in Photosystem II: Evaluation of the DFT/B3LYP Level of Theory. *J. Inorg. Biochem.* **2006**, *100*, 786−800.

(23) Sproviero, E. M.; Gascon, J. A.; McEvoy, J. P.; Brudvig, G. W.; Batista, V. S. QM/MM Models of the O_2-Evolving Complex of Photosystem II. *J. Chem. Theory Comput.* **2006**, *2*, 1119−1134.

(24) Wang, T.; Brudvig, G.; Batista, V. S. Characterization of Proton Coupled Electron Transfer in a Biomimetic Oxomanganese Complex: Evaluation of the DFT B3LYP Level of Theory. *J. Chem. Theory Comput.* **2010**, *6*, 755−760.

(25) Wang, T.; Brudvig, G. W.; Batista, V. S. Study of Proton Coupled Electron Transfer in a Biomimetic Dimanganese Water Oxidation Catalyst with Terminal Water Ligands. *J. Chem. Theory Comput.* **2010**, *6*, 2395−2401.

(26) Sproviero, E. M.; McEvoy, J. P.; Gascon, J. A.; Brudvig, G. W.; Batista, V. S. Computational insights into the O_2-Evolving Complex of Photosystem II. *Photosynth. Res.* **2008**, *97*, 91−114.

(27) Ames, W.; Pantazis, D. A.; Krewald, V.; Cox, N.; Messinger, J.; Lubitz, W.; Neese, F. Theoretical Evaluation of Structural Models of the S_2 State in the Oxygen Evolving Complex of Photosystem II: Protonation States and Magnetic Interactions. *J. Am. Chem. Soc.* **2011**, *133*, 19743−19757.

(28) Neese, F. Quantum Chemical Calculations of Spectroscopic Properties of Metalloprotenis and Model Compounds: EPR and Mossbauer Properties. *Curr. Opin. Chem. Biol.* **2003**, *7*, 125−135.

(29) Pantazis, D. A.; Orio, M.; Petrenko, T.; Zein, S.; Bill, E.; Lubitz, W.; Messinger, J.; Neese, F. A New Quantum Chemical Approach to the Magnetic Properties of Oligonuclear Transition-Metal Complexes: Application to a Model for the Tetranuclear Manganese Cluster of Photosystem II. *Chem.—Eur. J.* **2009**, *15*, 5108−5123.

(30) Siegbahn, P. E. Modeling aspects of Mechanisms for Reactions Catalyzed by Metalloenzymes. *J. Comput. Chem.* **2001**, *22*, 1634−1645.

(31) Siegbahn, P. E. Mechanisms of Metalloenzymes Studied by Quantum Chemical Methods. *Q. Rev. Biophys.* **2003**, *36*, 91−145.

(32) Siegbahn, P. E. A Comparison of the Thermodynamics of O-O Cleavage for Dicopper Complexes in Enzymes and Synthetic Systems. *J. Biol. Inorg. Chem.* **2003**, *8*, 577−585.

(33) Siegbahn, P. E.; Blomberg, M. R. Transistion-Metal Systems in Biochemistry Studied by High-Accuracy Quantum Chemical Methods. *Chem. Rev.* **2000**, *100*, 421−437.

(34) Siegbahn, P. E. M. A Quantum Chemical Study of the Mechanism of Manganese Catalase. *Theor. Chem. Acc.* **2001**, *105*, 197−206.

(35) Siegbahn, P. E. M.; Blomberg, M. R. A. Density Functional Theory of Biologically Relevant Metal Centers. *Annu. Rev. Phys. Chem.* **1999**, *50*, 221−249.

(36) Siegbahn, P. E. M.; Crabtree, R. H. Manganese Oxyl Radical Intermediates and O-O Bond Formation in Photosynthetic Oxygen Evolution and a Proposed Role for the Calcium Cofactor in Photosystem II. *J. Am. Chem. Soc.* **1999**, *121*, 117−127.

(37) Siegbahn, P. E. M.; Lundberg, M. The Mechanism for Dioxygen Formation in PSII Studied by Quantum Chemical Methods. *Photochem. Photobiol. Sci.* **2005**, *4*, 1035−1043.

(38) Luo, S.; Rivalta, I.; Batista, V.; Truhlar, D. G. Noncollinear Spins Explain the Low Spin State of a Biomimetic Oxomanganese Synthetic Trimer Inspired by the Oxygen Evolving Complex of Photosystem II. *J. Phys. Chem. Lett.* **2011**, *2*, 2629−2633.

(39) Hegarty, D.; Robb, M. A. Application of Unitary Group-Methods to Configuration-Interaction Calculations. *Mol. Phys.* **1979**, *38*, 1795−1812.

(40) Yamamoto, N.; Vreven, T.; Robb, M. A.; Frisch, M. J.; Schlegel, H. B. A Direct Derivative MC-SCF Procedure. *Chem. Phys. Lett.* **1996**, *250*, 373−378.

(41) Song, Y.; Mao, J.; Gunner, M. R. MCCE2: Improving Protein pK_a Calculations with Extensive Side Chain Rotamer Sampling. *J. Comput. Chem.* **2009**, *30*, 2231−2247.

(42) Ishikita, H.; Loll, B.; Biesiadka, J.; Saenger, W.; Knapp, E. W. Redox Potentials of Chlorophylls in the Photosystem II Reaction Center. *Biochemistry* **2005**, *44*, 4118−4124.

(43) Rabenstein, B.; Ullmann, G. M.; Knapp, E.-W. Calculation of Protonation Patterns in Proteins with Structural Relaxation and Molecular Ensembles-Application to the Photosynthetic Reaction Center. *Eur. Biophys. J.* **1998**, *27*, 626−637.

(44) Alexov, E.; Gunner, M. R. Calculated Protein and Proton Motions Coupled to Electron Transfer: Electron Transfer from Q_A^- to Q_B in Bacterial Photosynthetic Reaction Centers. *Biochemistry* **1999**, *38*, 8254−8270.

(45) Gunner, M. R.; Mao, J.; Song, Y.; Kim, J. Factors Influencing Energetics of Electron and Proton Transfers in Proteins. What Can Be Learned from Calculations. *Biochim. Biophys. Acta* **2006**, *1757*, 942−968.

(46) Rocchia, W.; Alexov, E.; Honig, B. Extending the Applicability of the Nonlinear Poisson-Boltzmann Equation: Multiple Dielectric Constants and Multivalent Ions. *J. Phys. Chem. B* **2001**, *105*, 6507−6514.

(47) Claire, W.; Finn, K. L.; Brian, N. F. Di-tz-oxo-bis[bis(bipyridine-N,N′)- Manganese(III,IV)] Triperchlorate Bis(nitrobenzene) Hemihydrate. *Acta Crystallogr., Sect. A* **1998**, *C54*, 1797−1799.

(48) Limburg, J.; Vrettos, J. S.; Liable-Sands, L. M.; Rheingold, A. L.; Crabtree, R. H.; Brudvig, G. W. A Functional Model for O-O Bond Formation by the O_2-Evolving Complex in Photosystem II. *Science* **1999**, *283*, 1524−1527.

(49) Gohdes, J. W.; Armstrong, W. H. *Inorg. Chem.* **1992**, *31*, 368−373.

(50) Hay, P. J.; Wadt, W. R. Ab Initio Effective Core Potentials for Molecular Calculations. Potentials for the Transition Metal Atoms Sc to Hg. *J. Chem. Phys.* **1985**, *82*, 270−283.

(51) Petersson, G. A.; Al-Laham, M. A. A complete basis set model chemistry. II. Open-shell systems and the total energies of the first-row atoms. *J. Chem. Phys.* **1991**, *94*, 6081−6090.

(52) Schmidt, M. W.; K., K. B.; Boatz, J. A.; Elbert, S. T.; Gordon, M. S.; Jensen, J. A.; Koseki, S.; Matsunaga, N.; Nguyen, K. A.; Su, S.; Windus, T. L.; Dupuis, M.; Montgomery, J. A. General Atomic and Molecular Electronic Structure System. *J. Comput. Chem.* **1993**, *14*, 1347−1363.

(53) *Jaguar 6.5*; Schrodinger, LLC: Portland, OR, 2005.

(54) Frisch, M. J.; Trucks, G. W.; Schlegel, H. B.; Scuseria, G. E.; Robb, M. A.; Cheeseman, J. R.; Scalmani, G.; Barone, V.; Mennucci, B.; Petersson, G. A.; et al. *Gaussian 09*, Revision A.1; Gaussian Inc.: Wallingford, CT, 2009.

(55) Noodleman, L. Valence Bond Description of Anti-Ferromagnetic Coupling in Transition-Metal Dimers. *J. Chem. Phys.* **1981**, *74*, 5737−5743.

(56) Thorp, H. H.; Sarneski, J. E.; Brudvig, G. W.; Crabtree, R. H. Proton-Coupled Electron Transfer in $[(bpy)_2Mn(O)_2Mn(bpy)_2]^{3+}$. *J. Am. Chem. Soc.* **1989**, *111*, 9249−9250.

(57) Jorgensen, W. L. Transferable Intermolecular Potential Functions for Water, Alcohols, and Ethers. Application to Liquid Water. *J. Am. Chem. Soc.* **1981**, *103*, 335−340.

(58) Becke, A. D. Density-Functional Exchange-Energy Approximation with Correct Asymptotic Behavior. *Phys. Rev. A* **1988**, *38*, 3098−3100.

(59) Becke, A. D. Density-Functional Thermochemistry 0.2. The Effect of the Perdew-Wang Generalized-Gradient Correlation Correction. *J. Chem. Phys.* **1992**, *97*, 9173−9177.

(60) Becke, A. D. Density-Functional Thermochemistry 0.3. The Role of Exact Exchange. *J. Chem. Phys.* **1993**, *98*, 5648−5652.

(61) Dunning, T. H., Jr. Gaussian Basis Sets for use in Correlated Molecular Calculations. I. The Atoms Boron through Neon and Hydrogen. *J. Chem. Phys.* **1989**, *90*, 1007−1023.

(62) Cooper, S. R.; Calvin, M. Mixed Valence Interactions in di-mu-oxo Bridged Manganese Complexes. *J. Am. Chem. Soc.* **1977**, *99*, 6623−6630.

(63) Baldwin, M. J.; Pecoraro, V. L. Energetics of Proton-Coupled Electron Transfer in High-Valent $Mn_2(\mu\text{-}O)_2$ Systems: Models for Water Oxidation by the Oxygen-Evolving Complex of Photosystem II. *J. Am. Chem. Soc.* **1996**, *118*, 11325−11326.

(64) Richens, D. T. *The Chemistry of Aqua Ions: Synthesis, Structure, and Reactivity: A Tour Through the Periodic Table of the Elements*; Wiley: Chichester, U.K, 1997; p 8.

(65) Jeon, S.; Bruice, T. C. Redox Chemistry of Water-Soluble Iron, Manganese, and Chromium Metalloporphyrins and Acid-Base Behavior of Their Lyate Axial Ligands in Aqueous Solution: Influence of Electronic Effects. *Inorg. Chem.* **1992**, *31*, 4843−4848.

(66) Cady, C. W.; Shinopoulos, K. E.; Crabtree, R. H.; Brudvig, G. W. $[(H_2O)(terpy)Mn(mu\text{-}O)_2Mn(terpy)(OH_2)](NO_3)_3$ (terpy = 2,2′:6,2″-terpyridine) and Its Relevance to the Oxygen-Evolving Complex of Photosystem II Examined through pH Dependent Cyclic Voltammetry. *Dalton Trans.* **2010**, *39*, 3985−3989.

(67) Das, S.; Mukhopadhyay, S. Mechanistic Studies on Oxidation of Nitrite by a $\{Mn_3O_4\}^{4+}$ Core in Aqueous Acidic Media. *Dalton Trans.* **2007**, 2321−2327.

(68) Mao, J.; Hauser, K.; Gunner, M. R. How Cytochromes with Different Folds Control Heme Redox Potentials. *Biochemistry* **2003**, *42*, 9829−9840.

(69) Morrison, M. M.; Sawyer, D. T. Redox Reactions of di-mu-oxo Bridged Binuclear Manganese(IV) and -(III) Complexes. *J. Am. Chem. Soc.* **1976**, *99*, 257−258.

(70) Baldwin, M. J.; Gelasco, A.; Pecoraro, V. L. The Effect of Protonation on $[Mn(IV)(\mu_2\text{-}O)]_2$ Complexes. *Photosynth. Res.* **1993**, *38*, 303−308.

(71) Weatherly, S. C.; Yang, I. V.; Thorp, H. H. Proton-Coupled Electron Transfer in Duplex DNA: Driving Force Dependence and Isotope Effects on Electrocatalytic Oxidation of Guanine. *J. Am. Chem. Soc.* **2001**, *123*, 1236−1237.

(72) Kristjánsdóttir, S.; Norton, J. In *Transition Metal Hydrides*; Dedieu, A., Ed.; VCH Publishers: New York; 1992; pp 309−359.

(73) Umena, Y.; Kawakami, K.; Shen, J.-R; Kamiya, N. Crystal Structure of Oxygen-Evolving Photosystem II at 1.9 Angstrom Resolution. *Nature* **2011**, *473*, 55−60.

(74) Brudvig, G. W. Water Oxidation Chemistry of Photosystem II. *Philos. Trans. R. Soc., B* **2008**, *363*, 1211−1218; discussion, pp 1218−1219.

(75) Sproviero, E. M.; Gascon, J. A.; McEvoy, J. P.; Brudvig, G. W.; Batista, V. S. Quantum Mechanics/Molecular Mechanics Structural Models of the Oxygen-Evolving Complex of Photosystem II. *Curr. Opin. Struct. Biol.* **2007**, *17*, 173−180.

(76) Sproviero, E. M.; Gascon, J. A.; McEvoy, J. P.; Brudvig, G. W.; Batista, V. S. QM/MM Study of the Catalytic Cycle for Water Splitting in Photosystem II. *J. Am. Chem. Soc.* **2008**, *130*, 3428−3442.

(77) Sproviero, E. M.; Gascon, J. A.; McEvoy, J. P.; Brudvig, G. W.; Batista, V. S. A Model of the Oxygen-Evolving Center of Photosystem II Predicted by Structural Refinement based on EXAFS Simulations. *J. Am. Chem. Soc.* **2008**, *130*, 6728−6730.

(78) Rappaport, F.; Lavergne, J. Proton Release during Successive Oxidation Steps of the Photosynthetic Water Oxidation Process: Stoichiometries and pH Dependence. *Biochemistry* **1991**, *30*, 10004−10012.

(79) Milikisiyants, R.; Chatterjee, C. S.; Coates, F. M. K.; Kua, J.-R. S.; Lakshmi, K. V. The Structure and Activation of Substrate Water Molecules in the S_2 State of Photosystem II Studied by Hyperfine Sublevel Correlation Spectroscopy. *Energy Environ. Sci.* **2012**, *5*, 7747−7756.

(80) Rivalta, I.; Amin, M.; Luber, S.; Vassiliev, S.; Pokhrel, R.; Umena, Y.; Kawakami, K.; Shen, J. R.; Kamiya, N.; Bruce, D.; et al. Structural-Functional Role of Chloride in Photosystem II. *Biochemistry* **2011**, *50*, 6312−6315.

(81) Song, Y.; Gunner, M. R. Using Multi-Conformation Continuum Electrostatics to Compare Chloride Binding Motifs in alpha-Amylase, Human Serum Albumin, and Omp32. *J. Mol. Biol.* **2009**, *387*, 840−856.

(82) Miller, A. F.; Padmakumar, K.; Sorkin, D. L.; Karapetian, A.; Vance, C. K. Proton-Coupled Electron Transfer in Fe-Superoxide Dismutase and Mn-Superoxide Dismutase. *J. Inorg. Biochem.* **2003**, *93*, 71−83.

(83) Mullins, C. S.; Pecoraro, V. L. Reflections on Small Molecule Manganese Models that Seek to Mimic Photosynthetic Water Oxidation Chemistry. *Coord. Chem. Rev.* **2008**, *252*, 416−443.